A Modal Description of Dynamic Wake Meandering

Nicholas Hamilton,[a] Paula Doubrawa, Patrick Moriarty, Stefano Letizia, and Regis Thedin

National Renewable Energy Laboratory (NREL), Golden, Colorado, USA

(Dated: 25 September 2024)

Lidar scans from a nacelle-mounted measurement system provide time series of wake measurements during three different atmospheric inflow conditions, from which we describe the coherent turbulent structures that contribute to wake meandering through proper orthogonal decomposition. Subsets of modes are used to make low-order flow field reconstructions in a combinatorial sense, yielding more than 30,000 estimates of meandering for each of the inflow cases. A regression test using the range of reconstructed flow statistics identifies the modes that contribute most to the accurate description of wake meandering. Spectra defined from each mode coefficient time series highlight the dominant Strouhal number associated with each coherent turbulent structure, and suggest that the lowest ranking modes do not necessarily contribute most to the accurate representation of wake meandering. Instead, some modes appear to have no influence on meandering dynamics, and still others consistently detract from wake meandering represented in low-dimensional flow reconstructions. No consistent relationship is revealed between characteristic frequencies for each mode and for either the inflow or the lidar measurements, suggesting that a more complex relationship between wake and inflow turbulence may be needed to accurately describe wake meandering.

[a]Electronic mail: nicholas.hamilton@nrel.gov

I. INTRODUCTION

Wake meandering, characterized by large-scale, quasiperiodic, low-frequency oscillations of the entire wind turbine wake, plays a crucial role in wind turbine loads, controller set point uncertainty, and power quality. Meandering significantly impacts power production and fatigue loading of downstream turbines in wind farms[1–3]. Despite its importance, accurately representing wake meandering in numerical models remains challenging across all fidelities, making any additional characterization of the phenomenon valuable for improving wind farm performance and reliability.

Two prevailing hypotheses attempt to explain the origin of wake meandering. The externally driven hypothesis considers the wake's momentum deficit as a passive tracer advected by large-scale atmospheric turbulence[1]. This theory suggests that only turbulent structures larger than the rotor diameter significantly contribute to wake meandering[1,4–8].

Alternatively, the internally driven hypothesis proposes that dynamic interactions between turbulent structures within the wake itself, such as tip vortices and hub/root vortices, generate pressure fluctuations substantial enough to displace the wake[9–14]. Also within the internally-driven set of hypotheses is that wake meandering may result from a fundamental shear instability that can be excited by multiple mechanisms[15,16].

Our ability to measure wind turbine wakes in the field has improved tremendously over the past decade. Ten years ago, some of the first dynamic wake measurements were collected by modifying a prototype lidar originally designed for vertical conical scanning[17,18]. These early measurements, despite their limitations, were used to validate basic assumptions of the dynamic wake meandering (DWM) model. Today, lidar technology allows us to observe wake dynamics for wind turbines of any size, with the capability to scan in any direction spanwise and vertically, reach downstream distances on the order of kilometers, and capture wake meandering, trajectory, expansion, and large-scale turbulent structures[2].

Nacelle-mounted lidars have emerged as a powerful tool for real-time characterization of inflow and wakes of utility-scale wind turbines[19]. These instruments offer unique capabilities for wind energy research, including real-time measurements for turbine and farm control, long-term performance assessment, high-resolution data assimilation for numerical simulations, and detailed wake characterization[18,20–26]. provide better characterization of the wind resource at relevant heights and allow effortless steering onto the wind direction for yaw-

controlled turbines. Despite their significant potential, barriers still exist in assimilating technology into wind energy industrial standards, partly due to the lack of consolidated scan design strategies and data processing techniques[27,28]. This review aims to provide a detailed account of applications and guidance for researchers using lidars and lidar data in wind energy research.

Several recent studies leverage modern lidar technology to characterize turbulence in the wake. Depending on the instrument deployed, lidars typically measure in vertical planes at fixed downstream distances[25,29,30], or in horizontal planes perpendicular to the rotor at hub height[31,32]. These recent, lidar-based studies have primarily looked at the temporal evolution of turbulence by identifying the wake within each scan and tracking its centerline position over time. The centerline is then used to quantify wake meandering for the sake of wake characterization[29] or model validation[25].[33,34]

To investigate under what conditions we can expect the internally-driven hypothesis to be the dominant mechanism driving wake meandering, we employ Proper Orthogonal Decomposition (POD). This method is well-suited for identifying coherent turbulence structures in flow fields[35] and has been applied to wind fields for over fifteen years[36–40]. POD seeks the variance-maximizing structures that describe the turbulent kinetic energy in the flow, making it an ideal tool for quantifying potential meandering-inducing structures in the wake. Our approach involves developing a reduced-order model (ROM) using the POD-derived structures. If these structures are shown to contribute significantly to wake meandering, the ROM should reproduce the meandering behavior seen in the measurement data to a high level of fidelity. Conversely, a ROM developed without these structures should fail to accurately reproduce wake meandering.

Through the use of POD, we will estimate the meandering length scales and frequencies in our dataset and relate them to DWM modeling assumptions. The body of past experimental and numerical work typically characterizes the meandering frequency (f_s) in the context of a Strouhal number, $St = f_s D/U_{\text{hub}}$ defined in terms of the wind turbine rotor diameter (D) and hub-height inflow velocity (U_{hub}). Meandering frequencies are typically reported in the range of $St = 0.1 - -0.35$[2,41,42], both in laboratory and field observations. If the internally-driven hypothesis for wake meandering is correct, the modes that contribute most to meandering should have characteristic frequencies higher than the inflow Strouhal number. Conversely, cases where the externally driven hypothesis is correct should favor structures

with frequencies below the inflow Strouhal number.

DWM models[1] consider only the inflow forcing, assuming the momentum deficit and wake center to advect as passive tracers in a background flow. Typically, this effect is considered by applying a low-pass filter to the turbulent inflow such that only structures that exceed a certain minimum length scale influence wake motion. This cut-off length scale is often set to twice the instantaneous wake diameter ($2D_w$[1,8]) or simply as twice the rotor diameter ($2D$) in many impletementatinos[43,44].

By combining advanced measurement techniques with sophisticated data analysis methods, we seek to develop an understanding of wake meandering across a wide range of atmospheric conditions. We relate and its impact on wind farm performance, ultimately contributing to the optimization of wind energy production and turbine longevity.

II. METHODS

A. Wake meandering

Wake meandering is quantified in this work through the dynamics of transverse coordinate of the wake center (μ), which we estimate by fitting a Gaussian profile to the momentum deficit derived from the lidar scans. The velocity deficit is defined as,

$$\tilde{u}(x,y,t) = 1 - \frac{u(x,y,t)}{U_{\text{hub}}(t)} \tag{1}$$

In Eq. (1), u represents the line-of-sight velocity measurement from the lidar. Because our data are collected in horizontal planes at hub height, we only consider lateral movements of the wake center along the y direction at a fixed height above ground $z = z_{hub}$. The wake center is detected through a least-squares fit of a Gaussian function to the observed U by the lidar at each downstream location and for each time.

$$\tilde{u}(x,y,t) = A \exp \frac{1}{2} \left[\frac{y - \mu(x,t)}{\sigma(x,t)} \right]^2 + C \tag{2}$$

In Eq. (2), the peak momentum deficit is denoted as A, the standard deviation corresponding to wake width is σ, and the lateral wake center is μ. An offset term, C, is included in the function, although it is typically a relatively small value, $-1 \lesssim C \lesssim 1$.

B. Snapshot proper orthogonal decomposition

Proper Orthogonal Decomposition (POD), also known as Principal Component Analysis (PCA) or Karhunen-Loève decomposition, has been widely used in fluid dynamics for identifying coherent structures and reducing the dimensionality of complex flow fields[35]. However, its application to data in polar coordinates, as is more natural for scanning lidar observations, presents unique challenges that necessitate a careful reconsideration of the method's foundational elements.

Snapshot POD begins with a sequence of observation $\mathbf{x}_k{}_{k=1}^{m}$, where each $\mathbf{x}_k \in \mathbb{R}^n$ represents the state of the system at time t_k. POD seeks an orthogonal basis that optimally represents the data in terms of captured variance.

When dealing with data in polar coordinates, the standard Euclidean inner product implicit in this formulation becomes inadequate. The varying cell sizes in a polar grid lead to an inherent bias, overemphasizing contributions from larger radii. To address this, we modify the standard POD algorithm to incorporate a physically appropriate inner product for polar coordinates.

With $\mathbf{x}(r, \theta)$ representing the line-of-sight velocity (state) vector in polar coordinates, we define a weighted inner product as,

$$\langle \mathbf{x}, \mathbf{y} \rangle_W = \int_0^{2\pi} \int_0^R \mathbf{x}(r, \theta) \cdot \mathbf{y}(r, \theta)\, r\, dr\, d\theta \tag{3}$$

For discrete data on a polar grid with spacing Δr and $\Delta\theta$ in the radial and azimuthal directions, resepectively, Eq. (3) becomes,

$$\langle \mathbf{x}, \mathbf{y} \rangle_W = \sum_{i=1}^{N_r} \sum_{j=1}^{N_\theta} \mathbf{x}(r_i, \theta_j) \cdot \mathbf{y}(r_i, \theta_j)\, r_i\, \Delta r\, \Delta\theta \tag{4}$$

The inner product in Eq. (4) can be represented by a diagonal weight matrix $\mathbf{W}$:

$$\mathbf{W} = \mathrm{diag}(r_1, r_1, ..., r_1, r_2, r_2, ..., r_2, ..., r_{N_r}, ..., r_{N_r}) \Delta r \Delta\theta \tag{5}$$

where each r_i is repeated N_θ times.

The new inner product is incorporated into the POD algorithm by modifying correlation matrix to account for the weights described by Eq. (5) as,

$$\mathbf{C} = \frac{1}{m} \mathbf{X}' \mathbf{W} \mathbf{X} \tag{6}$$

The POD modes are then obtained by solving the eigenvalue problem in the standard fashion,

$$\mathbf{C}\mathbf{v}_i = \lambda_i \mathbf{v}_i \tag{7}$$

where λ_i are the eigenvalues and $\mathbf{v}_i$ are the corresponding eigenvectors. The POD modes ϕ_i are then reconstructed as:

$$\phi_i = \frac{1}{\sqrt{\lambda_i}} \mathbf{X}\mathbf{v}_i \tag{8}$$

This formulation ensures that the POD modes accurately reflect the true spatial scales and turbulent kinetic energy of the flow structures in polar coordinates, without bias towards structures at larger radii.

The proposed modification maintains the core principles of POD while adapting it to the geometric constraints of polar coordinate systems. This approach aligns with the broader perspective, advocated by Holmes[45], that the choice of inner product in modal decompositions should reflect the physics of the problem at hand. By incorporating an inner product motivated by the polar description of the state vector, we extend the applicability of POD to a wider class of fluid dynamics problems, particularly those naturally described in polar or cylindrical coordinates, such as rotating flows, pipe flows, and atmospheric phenomena.

The key requirement for an inner product is that it must satisfy the following properties for all observations in the vector space:

1. Conjugate symmetry: $\langle u, v \rangle = \langle v, u \rangle^*$

2. Linearity in the second argument: $\langle u, av + bw \rangle = a\langle u, v \rangle + b\langle u, w \rangle$

3. Positive-definiteness: $\langle u, u \rangle \geq 0$, and $\langle u, u \rangle = 0$ if and only if $u = 0$

The inner product developed here satisfies these properties, justified by the fact that it correctly accounts for the non-uniform spacing of the polar grid. The factor r in the integrand (or r_i in the discrete sum in Eq. (4)) compensates for the increasing arc length at larger radii, ensuring that regions of the flow field are weighted proportionally to their actual physical area.

C. Reconstruction

The approach to velocity field reconstruction used in this work relies on the nature of the POD to organize input system dynamics into coherent structures. We develop a combina-

torial approach to reduced order modeling to identify the turbulent structure (POD modes, ϕ_i) that contribute most to wake meandering. Each combination of modes was determined by selecting k of the first N_r modes, where $k \in [3, ..., 15]$ and $N_r = 15$ was determined by requiring at least 85% of the TKE represented in the observational basis for each case. Flow fields reconstructed with each unique combination of modes were then used to estimate wake meandering identically as for the lidar scans, described in **??** . In every ROM, the zeroth mode, ϕ_0, representing the mean flow, is also included. The total number of combinations for each dataset was $K = \sum_{k=3}^{15} \binom{N_r}{k} + 1 = 16279$. Fig. 1 shows the number of combinations tested for each value of k.

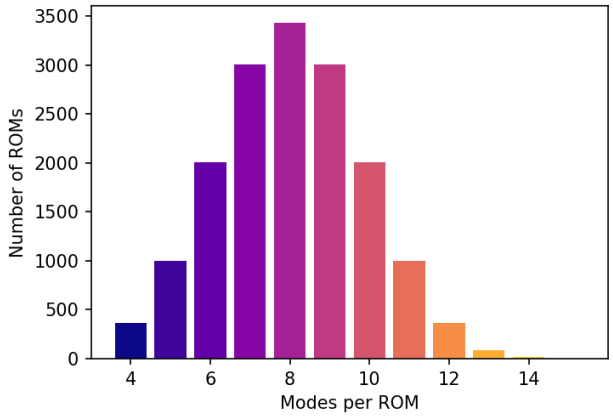

FIG. 1: l number of mode combinations used to reconstruct the flow field for a given maximum number of modes considered (k). For all cases, only modes 1 through 15 are considered ($N_r = 15$).

For each ROM, velocity fields are reconstruction from the truncated basis, summing over selected mode indices, rather than a sequential set up to a maximum. For each combination $I = \binom{N}{k}$, the reconstructed velocity field is,

$$\hat{u}(\boldsymbol{x}, t) = \sum_{i \in I} a_i(t) \Phi^{(i)}(\boldsymbol{x}) \tag{9}$$

where the index i may take only the values included in a particular combination of modes and the hat notation indicates a low-dimensional representation of the velocity field. In Eq. (9), the velocity field and modal basis have been denoted as scalars, as only the streamwise component of velocity is considered.

III. DATA

This work makes use of nacelle-mounted scanning lidar data from two recent DOE-funded field campaigns. The American WAKE ExperimeNt (AWAKEN[46]) is a multi-institutional field campaign designed to gather critical data on wind farm-atmosphere interactions, which contribute to uncertainty in wind plant performance models. These data will help validate and improve models, ultimately reducing uncertainty and increasing wind energy profitability. Observations from 13 ground-based locations and five wind turbines in Northern Oklahoma will be made publicly available to advance wind energy science and improve system reliability. Within the scope of this work, data sets from several sources in the AWAKEN Project have been considered. **NEED An AWAKEN CITATION, when will the JRSE paper be done?**

Atmospheric conditions were characterized through a combination of metrics derived from a surface flux station[47] and a meteorological tower[48] located at site A1. The surface flux station features a Gill R3-50 sonic anemometer mounted on a 4-meter-high tripod, recording data continuously at a 20 Hz rate. Data acquisition used software originally developed by Argonne National Laboratory for the ARM ECOR system in 2003, which was adapted for the AWAKEN project to work with Gill Sonic R3 series anemometers[49]. Sensible heat flux and momentum flux were processed into data at 30 minute resolution, assuming a constant relative humidity of 50% due to the absence of real-time humidity measurements. Hub-height wind speed and wind direction were recorded with a Thies 3D Ultrasonic anemometer. Turbulence intensity was estimated as a 10-min rolling calculation of the standard deviation of wind speed divided by mean wind speed in the same period. Wind directions were limited to a sector ranging from 170° to 200°, corresponding to the peak of the wind rose shown in Fig. 2. This also limited times when the wake from a neighboring turbine were visible in the data.

SCADA information from from Turbine H05 at the King Plains Wind Plant were used also used to select cases from the population of sets. Turbine H05 is located next to the main inflow site and hosted the nacelle-mounted scanning lidar used for wake observations.

The Rotor Aerodynamics, Aeroelastics, and Wake (RAAW) project is a field campaign designed to study the performance of modern flexible rotor wind turbines. Changes in tur-

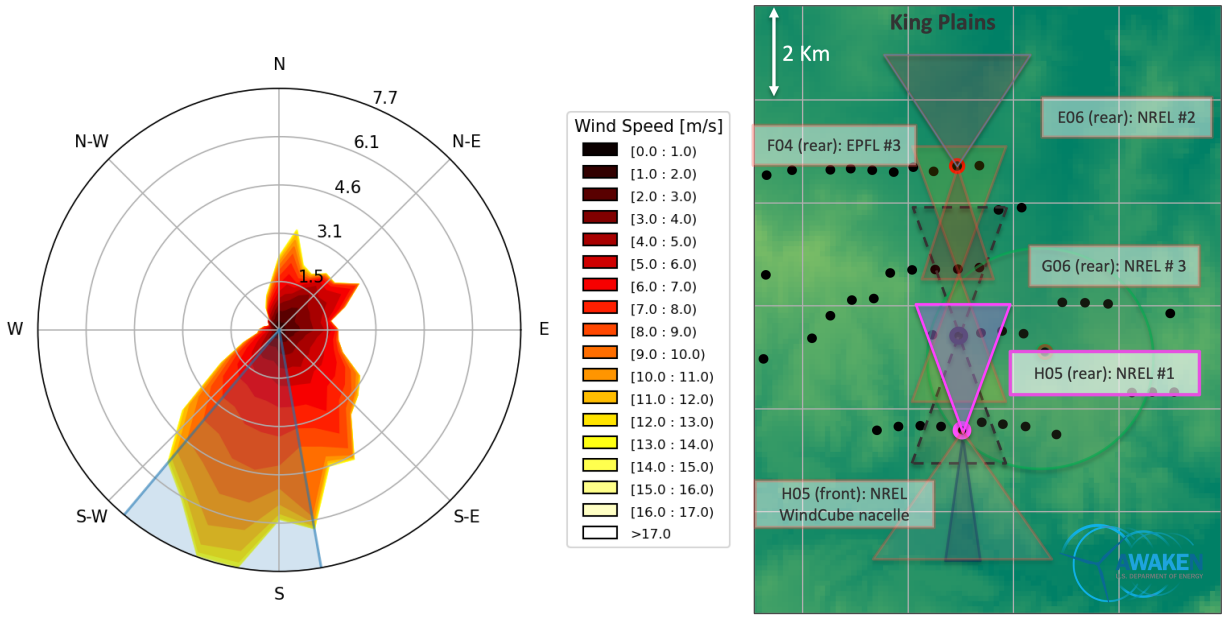

FIG. 2: Wind rose (left) and high-level schematic (right) of the AWAKEN project.

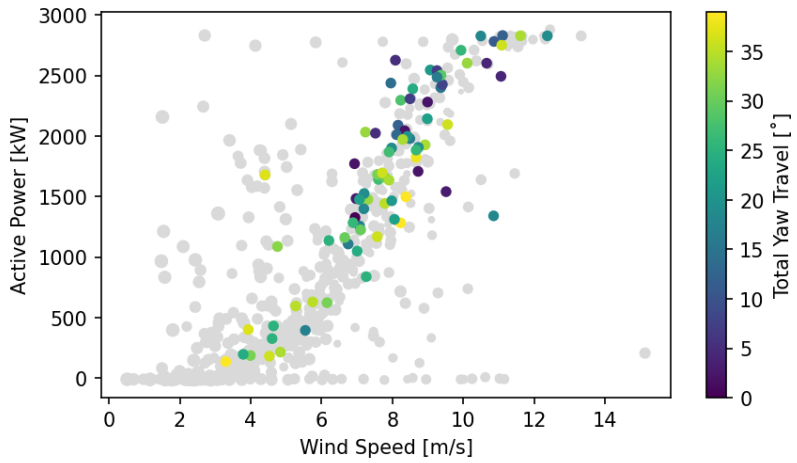

FIG. 3: Power curve from turbine H05 at the King Plains Wind Plant. All available cases are shown with gray points, cases selected for analysis in the current work are colored by the total yaw travel of the turbine during the measurement period.

bine design, including larger rotors and increased flexibility, have outpaced current models, leading to performance discrepancies and the need for validation with new experimental data. RAAW aims to fill this gap by providing detailed, time-dependent measurements of the inflow, turbine response, and wake, enabling better model validation and improved understanding of turbine behavior. **NEED A RAAW CITATION, when will the report**

be done?

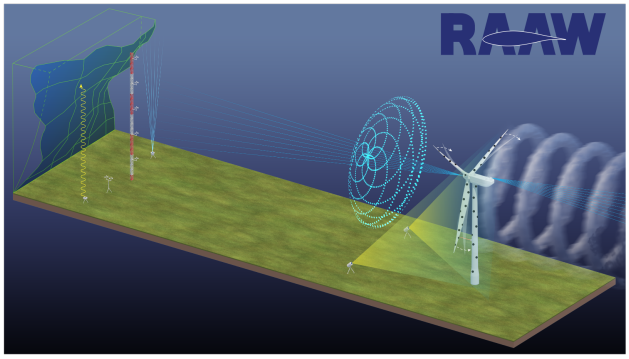

FIG. 4: high-level schematic (right) of the RAAW project showing the wind turbine, met tower, and associated instrumentation.

Both the RAAW and the AWAKEN project feature GE 2.8 MW turbines with 127 m rotor diameters. The RAAW project made use of the prototype/R&D turbine located in Lubbock, Tx, that had a hub height of 120 m. In the AWAKEN project, the turbines are production-run GE2.8-127 turbines with a hub height of 88.5 m.

Halo Photonics Doppler scanning lidars were positioned on the aft sections of the nacelles of the turbines of both projects and were configured for a variety of measurement strategies, including a plan-position indicator (PPI) scan optimized to measure the flucutating flow fields in the wake. Wake PPIs were designed using the LiSBOA tool[26], **sweeping XX degrees of azimuth per second convering a sector of XX degrees centered downstream of the turbine.** Lidar data were quality controlled using the **FIEXTA software** that includes the dynamic filtering methods outlined by Beck and Kühn[33]. Data are temporally upsampled considering local advection velocities and the time delays between successive beams at similar azimuth angles[34], producing line-of-sight velocity 'snapshots' at a temporal resolution of 1 second. Line of sight velocity is used in the subsequent analysis without transformation into Cartesian velocity vector components.

Meassurement cases combining lidar data sets and inflow measurements, were considered only after passing through the following filters:

1. Stuck/broken/defective sensors
2. Wind direction within the appropriate sector
3. Total yaw travel below 20°

4. Active power greater than 150 kW

5. Exclude cases with highest total variability

These quality control steps ensure that we consider only cases where all required measurements are reliable by eliminating cases where any data are missing or any sensors are fail to report reasonable observations. Because we rely on characteristics of the inflow to contextualize wind turbine wake meandering, we limit allowable wind directions to only the sectors for which the met towers and flux stations are located in the inflow to the turbine. For data from the AWAKEN project, this step also ensures that only the wake dynamics from the single turbine of interest are present in the lidar scans.

In both the RAAW and AWAKEN projects, the wind turbine is operated at a nominal control point. As such, the turbine is free to yaw the rotor to optimally align with the incoming wind. Yaw activity is evident within the lidar scans as abrupt changes or sweeping movements of the wakes within the scanned sectors. Very few lidar scan periods are available in either experiment that are free from any yaw activity. For the following work, we consider only cases where the aggregate yaw travel is less than 20°.

While we are interested in describing wake meandering under a wide range of atmospheric conditions, including a broad range of inflow wind speeds, we disallow any cases where the turbine is generating less than 150 kW. The lower limit on power production ensures that the turbine is operating within region 2 of the power curve and that a wake will be evident in the lidar data.

As a final quality control step, we calculate the total variation of the combined atmospheric state and operational state of the turbine following the method outlined in Hamilton[50]. The total variation is defined as the determinate of the covariance matrix relating inflow wind speed, wind direction, and turbulence intensity, as well as the turbine power production and nacelle position signals from the SCADA record. Cases where the total variation was greater than the 90^{th} percentile were excluded from further consideration. This step ensured that only statistically stationary conditions were taken under consideration, disallowing cases where the bulk atmospheric conditions change drastically during a lidar scan period or where a more significant control action was undertaken for the turbine.

The integral time scale of turbulent fluctuations in the inflow is calculated based on 20-Hz wind speed measurements collected with the sonic anemometer at 50 m height on the met

mast described above. The integral time scale, T, is defined as,

$$T = \int_0^{\tau|\rho=0.05} u'(t)u'(t+\tau)d\tau \tag{10}$$

where u is the mean wind speed during 30-min cases, and u' is the fluctuating component of the velocity signal. T is estimated as the integral of the autocorrelation, $\rho(\tau)$, which is a function only of the time lag, τ. A threshold of $\rho = 0.05$ is considered to calculate as the upper limit of the integral, rather than zero crossing point.[51,52] The integral time scale for each case was calculated from the horizontal wind speed by the respective met towers.

Figure 5 shows the distribution of inflow wind speed, U_∞, integral time scale, T, and inflow Strouhal number, St_{in} for each of the 71 cases from the combined RAAW aand AWAKEN experiments. The integral time scales, T, are taken as the characteristic period of the fluctuation in the velocity field and are used to define the characteristic frequency of turbulent fluctuations in the discussion of meandering frequencies.

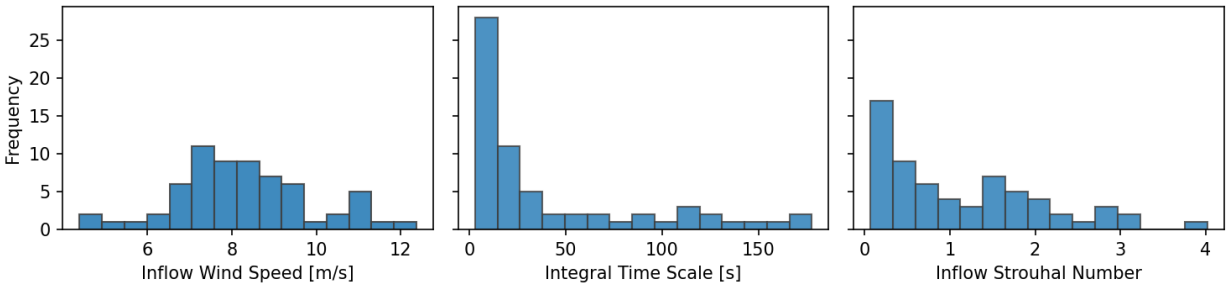

FIG. 5: Distributions of the average inflow wind speed, U_∞, integral time scale, T, and Strouhal Number, St_{in}, for each case.

IV. RESULTS

The full analysis we undertake in the current work is quite complex. We present results in this section for a single dataset to illustrate the full workflow, then contextualize the high-level relationships for all 71 cases later on.

$$P_{\mu\mu}(f) = \frac{1}{L}\sum_{k=1}^{K}\frac{1}{N}\left|\sum_{n=1}^{N}\mu_k(n)e^{-i2\pi fn/N}\right|^2 \tag{11}$$

where, K is the number of segments, $L = 512$ samples is the number of points in the FFT $N = 1,024$ is the length of each segment, $\mu_k(n)$ is the k-th segment of the time series. A

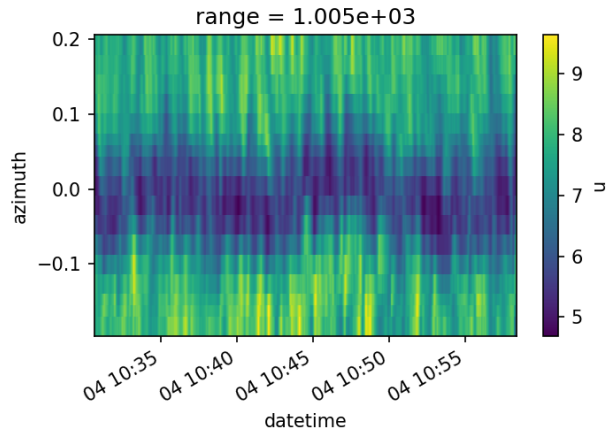

FIG. 6: Time-azimuth cross section of a line of sight velcoity from a lidar scan 1,005 m downstream of the lidar. The wake is shown in dark blue and background velocity in green/yellow.

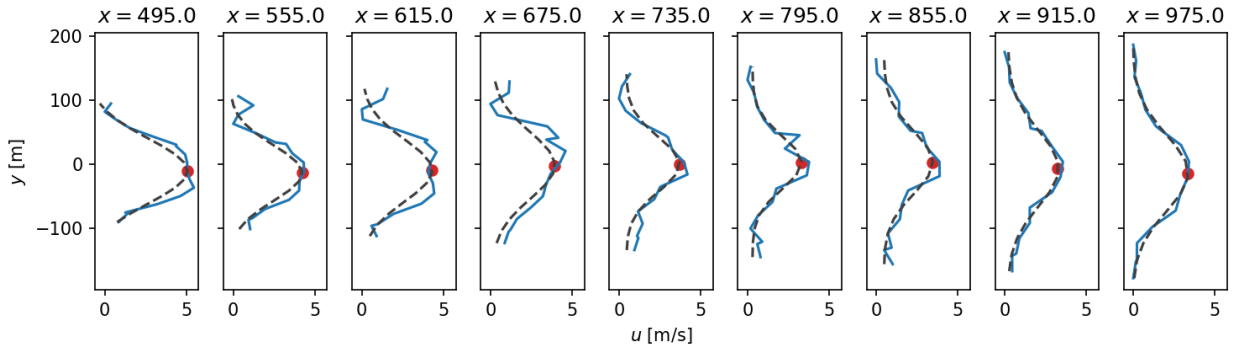

FIG. 7: Detected wake centers showing Guassian fit against momentum deficit. Blue lines indicate momentum deficit estimated from lidar scans, dashed line shows the fit Gaussian profile, red point is the detected wake center μ.

uniform window function is applied to each segment in the calculation of the PSDs. The frequency range for all spectra in the current work have been normalized with the average inflow velocity recorded by the met towers, U_∞, and the turbine's rotor diameter, D, as $f_{St} = f * D/U_\infty$

We use coherence Eq. (12) to quantify the similarity of wake center trajectories between the lidar scans and any of the ROMs.

$$\gamma^2(f) = \frac{|\mathcal{P}_{\mu\hat{\mu}_r}(f)|^2}{\mathcal{P}_{\mu\mu}(f)\mathcal{P}_{\hat{\mu}_r\hat{\mu}_r}(f)} \tag{12}$$

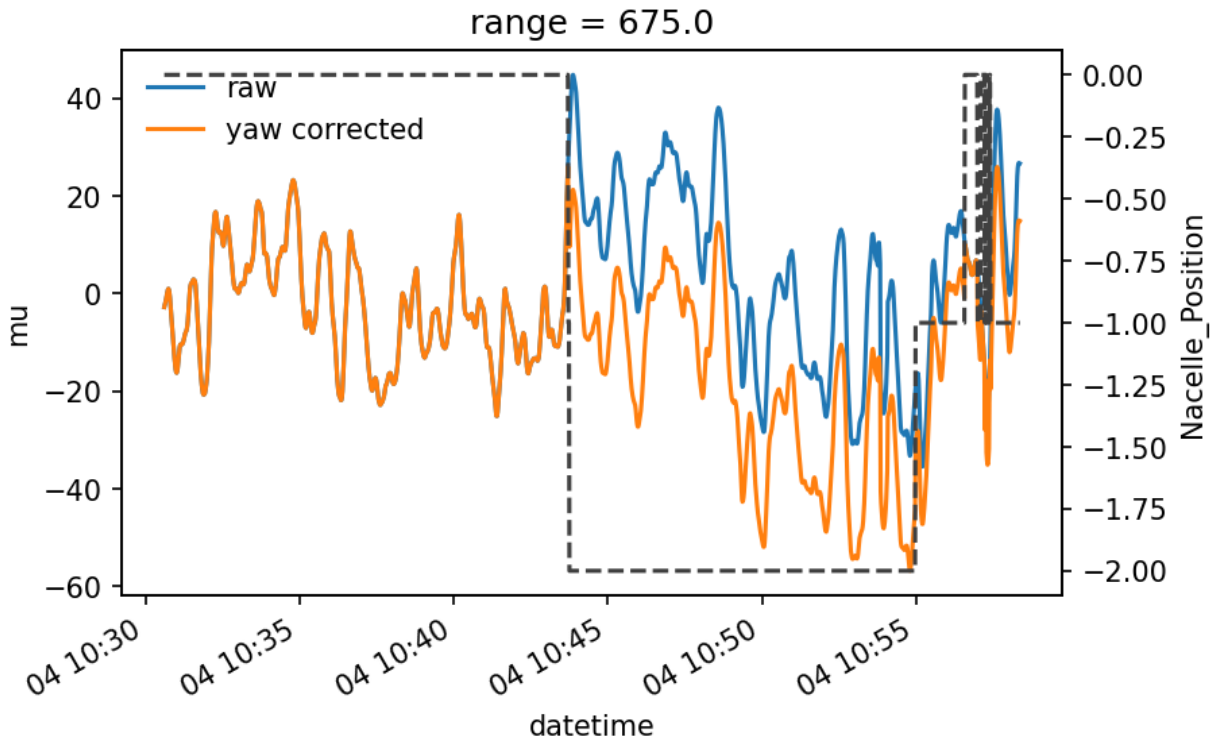

FIG. 8

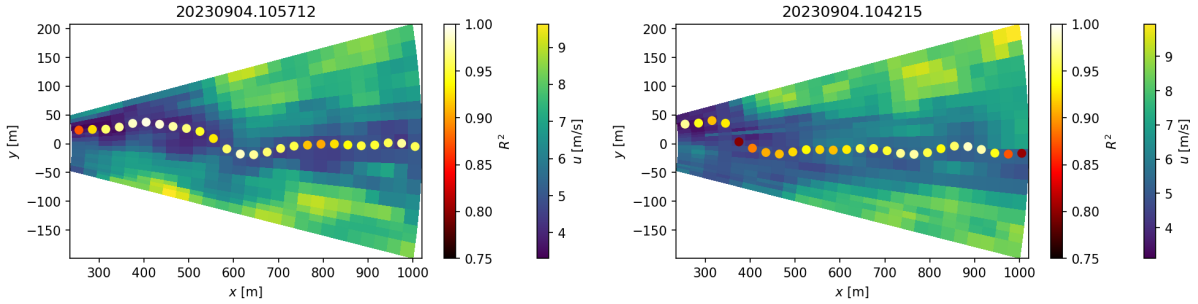

FIG. 9: Example lidar scans showing u overlaid with the fitted wake centers. Detected wake centers are colored by their respective coefficent of determination.

ACKNOWLEDGEMENTS

This work was authored in part by the National Renewable Energy Laboratory, operated by Alliance for Sustainable Energy, LLC, for the U.S. Department of Energy (DOE) under Contract No. DE-AC36-08GO28308. Funding provided by the U.S. Department of Energy Office of Energy Efficiency and Renewable Energy Wind Energy Technologies Office. The views expressed herein do not necessarily represent the views of the DOE or the U.S.

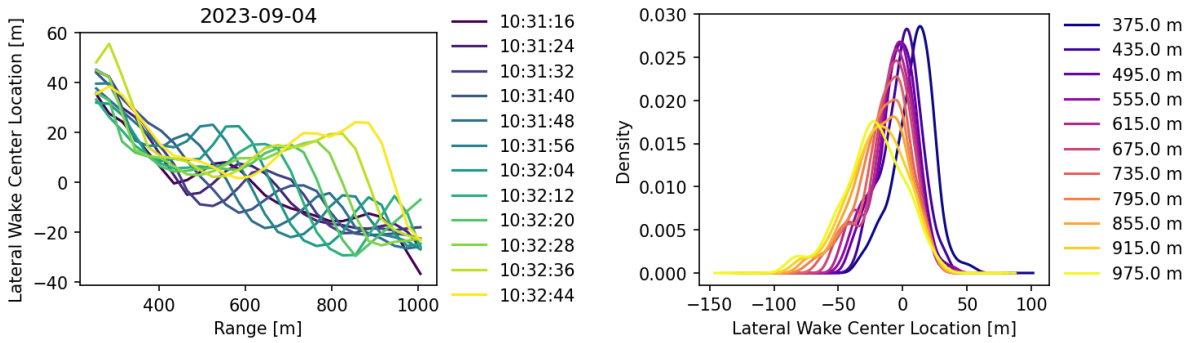

FIG. 10: Wake center trajectories for selected times (left) and kernal density estiamtes of wake centers by distance downstream of the lidar (right).

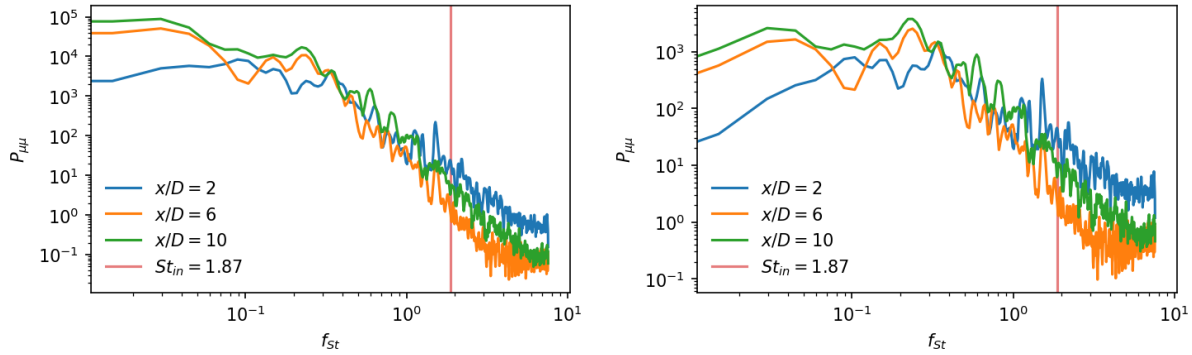

FIG. 11: PSDs (left) and premultiplied spectra (right) of detected wake centers from the lidar data at selected downstream distances.

REFERENCES

[1]G. C. Larsen, H. A. Madsen, K. Thomsen, and T. J. Larsen, "Wake meandering: a pragmatic approach," Wind Energy: An International Journal for Progress and Applications in Wind Power Conversion Technology **11**, 377–395 (2008).

[2]P. Brugger, M. Debnath, A. Scholbrock, P. Fleming, P. Moriarty, E. Simley, D. Jager, J. Roadman, M. Murphy, H. Zong, *et al.*, "Lidar measurements of yawed-wind-turbine

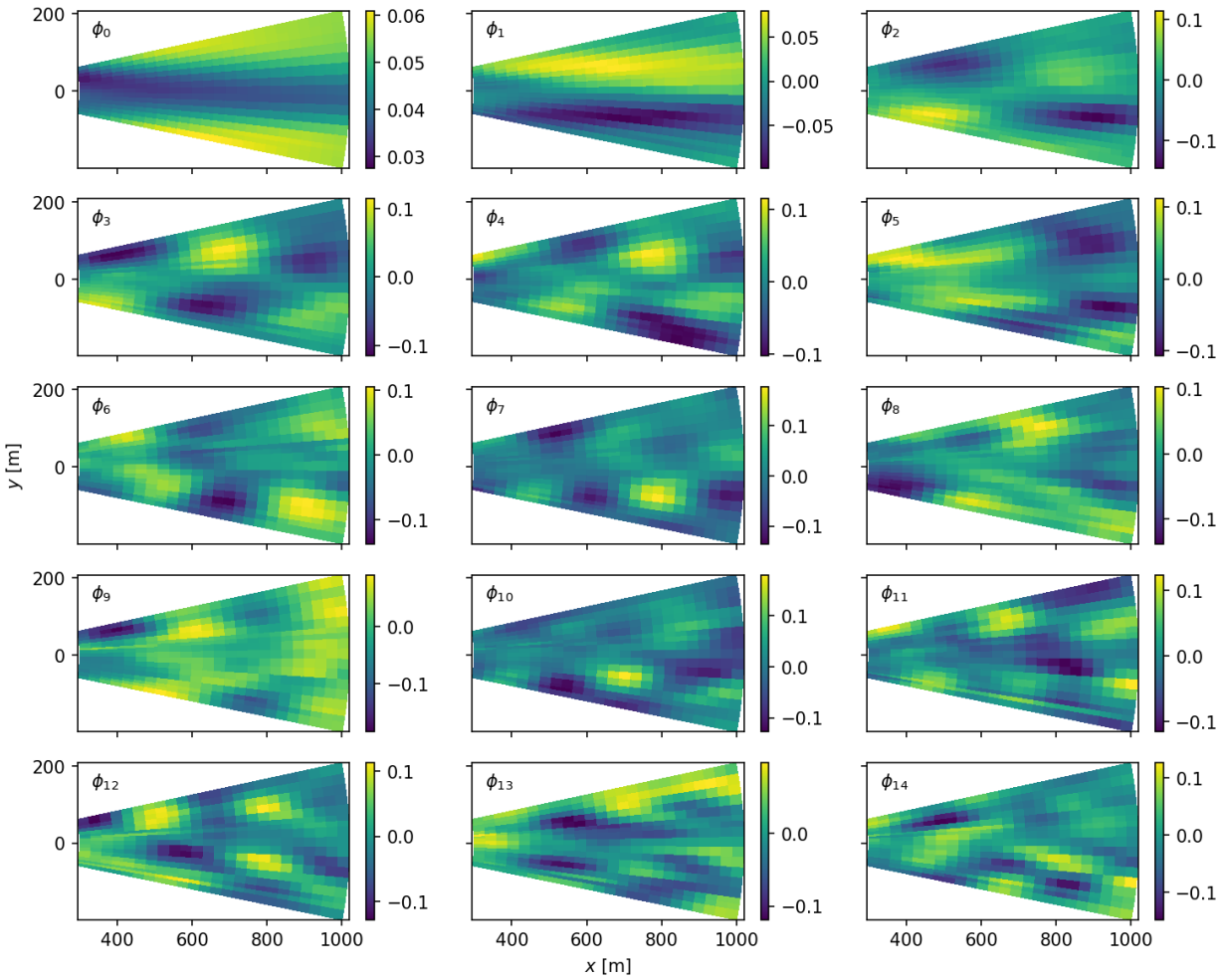

FIG. 12: POD modes from the example case on 2023-09-04 10:30 UTC.

wakes: characterization and validation of analytical models," Wind Energy Science **5**, 1253–1272 (2020).

[3]A. S. Wise and E. E. Bachynski, "Wake meandering effects on floating wind turbines," **23**, 1266–1285.

[4]G. Espana, S. Aubrun, S. Loyer, and P. Devinant, "Wind tunnel study of the wake meandering downstream of a modelled wind turbine as an effect of large scale turbulent eddies," Journal of Wind Engineering and Industrial Aerodynamics **101**, 24–33 (2012).

[5]R. W. Baker and S. N. Walker, "Wake velocity deficit measurements at the goodnoe hills mod-2 site: A summary of the 1982 and 1984 findings." Tech. Rep. (Oregon State Univ., Corvallis (USA). Wind Resources Assessment Lab., 1985).

[6]T. Zambrano and G. Gyatt, "Wake structure measurements at the mod-2 cluster test facilty at goodnoe hills, washington," IEE Proceedings A (Physical Science, Measurement and Instrumentation, Management and Education, Reviews) **130**, 562–565 (1983).

[7]G. C. Larsen, H. Aagaard Madsen, and F. Bingöl, "Dynamic wake meandering modeling," (2007).

[8]J. M. Jonkman, J. Annoni, G. Hayman, B. Jonkman, and A. Purkayastha, "Development of fast. farm: A new multi-physics engineering tool for wind-farm design and analysis," in *35th Wind Energy Symposium* (2017) p. 0454.

[9]D. Medici and P. H. Alfredsson, "Measurements behind model wind turbines: further evidence of wake meandering," Wind Energy: An International Journal for Progress and Applications in Wind Power Conversion Technology **11**, 211–217 (2008).

[10]V. Okulov and J. N. Sørensen, "Stability of helical tip vortices in a rotor far wake," Journal of Fluid Mechanics **576**, 1–25 (2007).

[11]V. L. Okulov, I. V. Naumov, R. F. Mikkelsen, I. K. Kabardin, and J. N. Sørensen, "A regular strouhal number for large-scale instability in the far wake of a rotor," Journal of Fluid Mechanics **747**, 369–380 (2014).

[12]K. B. Howard, A. Singh, F. Sotiropoulos, and M. Guala, "On the statistics of wind turbine wake meandering: An experimental investigation," Physics of Fluids **27**, 075103 (2015).

[13]D. Foti, X. Yang, M. Guala, and F. Sotiropoulos, "Wake meandering statistics of a model wind turbine: Insights gained by large eddy simulations," Physical Review Fluids **1**, 044407 (2016).

[14]D. Foti, X. Yang, F. Campagnolo, D. Maniaci, and F. Sotiropoulos, "Wake meandering of a model wind turbine operating in two different regimes," Physical Review Fluids **3**, 054607 (2018).

[15]S. J. Andersen, J. N. Sørensen, and R. Mikkelsen, "Simulation of the inherent turbulence and wake interaction inside an infinitely long row of wind turbines," Journal of Turbulence **14**, 1–24 (2013).

[16]Z. Li, G. Dong, and X. Yang, "Onset of wake meandering for a floating offshore wind turbine under side-to-side motion," **934**, A29.

[17]F. Bingöl, J. Mann, and G. C. Larsen, "Light detection and ranging measurements of wake dynamics part I: one-dimensional scanning," Wind Energy **13**, 51–61 (2010).

[18]J.-J. Trujillo, F. Bingöl, G. C. Larsen, J. Mann, and M. Kühn, "Light detection and ranging measurements of wake dynamics. Part II: two-dimensional scanning," Wind Energy **14**, 61–75 (2011).

[19]S. Letizia, P. Brugger, N. Bodini, R. Krishnamurthy, A. Scholbrock, E. Simley, F. Porté-Agel, N. Hamilton, P. Doubrawa, and P. Moriarty, "Characterization of wind turbine flow through nacelle-mounted lidars: a review," Frontiers in Mechanical Engineering **9**, 1261017 (2023).

[20]V.-M. Kumer, J. Reuder, B. Svardal, C. Sætre, and P. Eecen, "Characterisation of single wind turbine wakes with static and scanning wintwex-w lidar data," Energy Procedia **80**, 245–254 (2015).

[21]N. Bodini, D. Zardi, and J. K. Lundquist, "Three-dimensional structure of wind turbine wakes as measured by scanning lidar," Atmospheric Measurement Techniques **10**, 2881–2896 (2017).

[22]L. Zhan, S. Letizia, and G. Valerio Iungo, "Lidar measurements for an onshore wind farm: Wake variability for different incoming wind speeds and atmospheric stability regimes," Wind Energy **23**, 501–527 (2020).

[23]G. V. Iungo, Y.-T. Wu, and F. Porté-Agel, "Field measurements of wind turbine wakes with lidars," Journal of Atmospheric and Oceanic Technology **30**, 274–287 (2013).

[24]G. V. Iungo and F. Porté-Agel, "Volumetric lidar scanning of wind turbine wakes under convective and neutral atmospheric stability regimes," Journal of Atmospheric and Oceanic Technology **31**, 2035–2048 (2014).

[25]P. Doubrawa, E. W. Quon, L. A. Martinez-Tossas, K. Shaler, M. Debnath, N. Hamilton, T. G. Herges, D. Maniaci, C. L. Kelley, A. S. Hsieh, *et al.*, "Multimodel validation of single wakes in neutral and stratified atmospheric conditions," Wind Energy **23**, 2027–2055 (2020).

[26]S. Letizia, L. Zhan, and G. V. Iungo, "Lisboa (lidar statistical barnes objective analysis) for optimal design of lidar scans and retrieval of wind statistics–part 2: Applications to lidar measurements of wind turbine wakes," Atmospheric Measurement Techniques **14**, 2095–2113 (2021).

[27]A. Clifton, P. Clive, J. Gottschall, D. Schlipf, E. Simley, L. Simmons, D. Stein, D. Trabucchi, N. Vasiljevic, and I. Würth, "Iea wind task 32: Wind lidar identifying and mitigating barriers to the adoption of wind lidar," Remote Sensing **10**, 406 (2018).

[28]E. Simley, H. Fürst, F. Haizmann, and D. Schlipf, "Optimizing lidars for wind turbine control applications—results from the iea wind task 32 workshop," Remote Sensing **10**, 863 (2018).

[29]D. Conti, N. Dimitrov, A. Peña, and T. Herges, "Wind turbine wake characterization using the SpinnerLidar measurements," Journal of Physics: Conference Series **1618**, 062040 (2020).

[30]D. Conti, N. Dimitrov, A. Peña, and T. Herges, "Calibration and validation of the Dynamic Wake Meandering model Part I: Bayesian estimation of model parameters using SpinnerLidar-derived wake characteristics," Wind Energy Science Discussions , 1–39 (2021).

[31]I. Reinwardt, L. Schilling, P. Dalhoff, D. Steudel, and M. Breuer, "Dynamic wake meandering model calibration using nacelle-mounted lidar systems," Wind Energy Science **5**, 775–792 (2020).

[32]I. Reinwardt, L. Schilling, D. Steudel, N. Dimitrov, P. Dalhoff, and M. Breuer, "Validation of the dynamic wake meandering model with respect to loads and power production," Wind Energy Science **6**, 441–460 (2021).

[33]H. Beck and M. Kühn, "Dynamic Data Filtering of Long-Range Doppler LiDAR Wind Speed Measurements," **9**, 561 ().

[34]H. Beck and M. Kühn, "Temporal Up-Sampling of Planar Long-Range Doppler LiDAR Wind Speed Measurements Using Space-Time Conversion," **11**, 867 ().

[35]G. Berkooz, P. Holmes, and J. L. Lumley, "The proper orthogonal decomposition in the analysis of turbulent flows," Annual review of fluid mechanics **25**, 539–575 (1993).

[36]J. Spitler, S. Morton, J. Naughton, and W. Lindberg, "Initial Studies of Low-Order Turbulence Modeling of the Wind Turbine In-Flow Environment," in *42nd AIAA Aerospace Sciences Meeting and Exhibit* (American Institute of Aeronautics and Astronautics, 2004).

[37]K. Saranyasoontorn and L. Manuel, "Low-Dimensional Representations of Inflow Turbulence and Wind Turbine Response Using Proper Orthogonal Decomposition," Journal of Solar Energy Engineering **127**, 553–562 (2005).

[38]N. Hamilton, M. Tutkun, and R. B. Cal, "Wind turbine boundary layer arrays for cartesian and staggered configurations: Part II, low-dimensional representations via the proper orthogonal decomposition," Wind Energy **18**, 297–315 (2015).

[39]N. Hamilton, M. Tutkun, and R. B. Cal, "Low-order representations of the canonical wind turbine array boundary layer via double proper orthogonal decomposition," Physics of Fluids **28**, 025103 (2016).

[40]C. VerHulst and C. Meneveau, "Large eddy simulation study of the kinetic energy entrainment by energetic turbulent flow structures in large wind farms," Physics of Fluids **26**, 025113 (2014).

[41]N. Coudou, S. Buckingham, L. Bricteux, and J. van Beeck, "Experimental study on the wake meandering within a scale model wind farm subject to a wind-tunnel flow simulating an atmospheric boundary layer," Boundary-layer meteorology **167**, 77–98 (2018).

[42]M. Heisel, J. Hong, and M. Guala, "The spectral signature of wind turbine wake meandering: A wind tunnel and field-scale study," Wind Energy **21**, 715–731 (2018).

[43]K. Shaler, J. Jonkman, P. Doubrawa Moreira, and N. Hamilton, "Fast. farm response to varying wind inflow techniques," Tech. Rep. (National Renewable Energy Lab.(NREL), Golden, CO (United States), 2019).

[44]K. Shaler, J. Jonkman, and N. Hamilton, "Effects of inflow spatiotemporal discretization on wake meandering and turbine structural response using fast. farm," in *Journal of Physics: Conference Series*, Vol. 1256 (IOP Publishing, 2019) p. 012023.

[45]P. Holmes, *Turbulence, coherent structures, dynamical systems and symmetry* (Cambridge university press, 2012).

[46]P. Moriarty, N. Hamilton, M. Debnath, T. Herges, B. Isom, J. K. Lundquist, D. Maniaci, B. Naughton, R. Pauly, J. Roadman, *et al.*, "American wake experiment (awaken)," Tech. Rep. (Lawrence Livermore National Lab.(LLNL), Livermore, CA (United States . . . , 2020).

[47]Atmosphere to Electrons (A2e), "awaken/sa1.sonic.z01.b0," `https://a2e.energy.gov/data` (2024), maintained by A2e Data Archive and Portal for U.S. Department of Energy, Office of Energy Efficiency and Renewable Energy.

[48]Atmosphere to Electrons (A2e), "awaken/kp.met.z01.a0," `https://a2e.energy.gov/data` (2023), maintained by A2e Data Archive and Portal for U.S. Department of Energy, Office of Energy Efficiency and Renewable Energy.

[49]D. R. Cook, "Eddy correlation flux measurement system (ecor) instrument handbook," Tech. Rep. (DOE Office of Science Atmospheric Radiation Measurement (ARM) Program . . . , 2018).

[50]N. Hamilton, "Atmospheric condition identification in multivariate data through a metric for total variation," Atmospheric Measurement Techniques **13**, 1019–1032 (2020).

[51]E. Simley and L. Y. Pao, "A longitudinal spatial coherence model for wind evolution based on large-eddy simulation," in *2015 American Control Conference (ACC)* (2015) pp. 3708–3714.

[52]M. Debnath, P. Brugger, E. Simley, P. Doubrawa, N. Hamilton, A. Scholbrock, D. Jager, M. Murphy, J. Roadman, J. K. Lundquist, P. Fleming, F. Porté-Agel, and P. Moriarty, "Longitudinal coherence and short-term wind speed prediction based on a nacelle-mounted doppler lidar," Journal of Physics: Conference Series **1618**, 032051 (2020).